Journal of Molecular Catalysis A: Chemical 338 (2011) 71–83

Contents lists available at ScienceDirect

Journal of Molecular Catalysis A: Chemical

journal homepage: www.elsevier.com/locate/molcata

Oxidation of ethylbenzene using some recyclable cobalt nanocatalysts: The role of linker and electrochemical study

M. Arshadi [a], M. Ghiaci [a,*], A.A. Ensafi [a], H. Karimi-Maleh [a], Steven L. Suib [b]

[a] Department of Chemistry, Isfahan University of Technology, Isfahan 8415683111, Iran
[b] Department of Chemistry, University of Connecticut, Storrs, CN 06269-3060, USA

ARTICLE INFO

Article history:
Received 1 October 2010
Received in revised form 25 January 2011
Accepted 26 January 2011
Available online 5 March 2011

Keywords:
Cobalt
Ethylbenzene
Oxidation
Acetophenone
Carbon nanotubes
SiO_2–Al_2O_3

ABSTRACT

In this paper some Co(II)–Schiff base complexes were immobilized on SiO_2–Al_2O_3 mixed-oxide using two linkers with different flexibilities (3-aminopropyl and 2-aminoethyl-3-aminopropyl). The synthesized materials were characterized by FT-IR spectroscopy, UV–Vis, CHN elemental analysis, ICP-MS, EPR, SEM, TEM, cyclic voltammetry (CV) and electrochemical impedance spectroscopy (EIS). The catalytic activity of the heterogenized Co(II)–Schiff base complexes in the oxidation of ethylbenzene was studied without the need of any solvent, at 353 K, using *tert*-butyl hydroperoxide as oxygen source. The best catalyst has a higher catalytic activity (86%) and selectivity to acetophenone (99%) at TBHP/ethylbenzene molar ratio (1:1), and could be reused at least 4 times without significant loss in acetophenone yield, suggesting that no complex leaching took place under the reaction conditions. The electrochemical data about oxidation of the immobilized Co(II)–Schiff base complexes at the surface of multi-walled carbon nanotubes was also studied. The results indicate that the Co-complexes anchored on the modified SiO_2–Al_2O_3 mixed-oxide have an easily oxidizable environment, which led to higher catalytic activity and selectivity.

1. Introduction

Indeed, catalytic oxidation is the single most important technology for the conversion of hydrocarbons to industrially important oxygenated derivatives [1]. Selective oxidation of the C–H bonds in ethylbenzene is an attractive field as well as unsolved problem in chemistry. In this oxidation, the intermediate such as acetophenone is more susceptible to secondary oxidation reaction to the corresponding carboxylic acid which lowers the selectivity. Thus, the formation of ketone with high selectivity is more difficult. The production of acetophenone imparts high value addition, because it is used as intermediate for the manufacture of pharmaceuticals, resins, alcohols, esters, aldehydes and tear gas and is also used as a component in perfumery, and as a solvent for cellulose ethers.

Cobalt-based catalysts, due to their plausible potential as commercial catalysts, are the ones among the most investigated. In this regard Co(II) complexes are an important class of oxidants for this type of reactions and quite a number of studies have been conducted [2,3]. The current industrial production of acetophenone is *via* the oxidation of ethylbenzene with molecular oxygen using cobalt cycloalkanecarboxylate or cobalt acetate as catalyst in acetic acid solvent [4]. This method suffers from its corrosive and environmentally unfriendly nature. One of the major drawbacks of using organometallic compounds in homogenous solutions is the formation of μ-oxo dimers and other polymeric species which lead to irreversible catalyst deactivation. The problem has been avoided in principle by isolating the metal complexes from each other by immobilization through covalent bond on the solid supports. In recent years, encapsulation of metal complexes on the solid supports, typically zeolites and mixed oxides, have been extensively studied in an attempt to prepare isolated catalytically active centers that do not undergo rapid degradation as the homologous analogous [5,6]. Homogeneous and heterogeneous catalysts offer their own distinct advantages. Heterogeneous catalysts have an advantage that at the end of reaction the catalyst can be removed by simple filtration. In principle the product is un-contaminated with a transition metal or ligand and allows the catalyst to be recycled into the next reaction.

Recently there has been an increased interest in the development of clean and economical processes for the selective oxidation of ethylbenzene to higher-value added product acetophenone over both homogenous and especially heterogeneous cobalt-based catalysts [7–11]. As part of our continuing efforts directed toward the elucidation of the correlation between catalytic activity and electrochemical behavior of the synthesized heterogeneous complexes, we have further explored the behavior of the immobilized Co(II)–Schiff base complexes in a model reaction, i.e., the oxidation of ethylbenzene [12].

* Corresponding author. Tel.: +98 311 3913254; fax: +98 311 3912350.
E-mail address: mghiaci@cc.iut.ac.ir (M. Ghiaci).

1381-1169/$ – see front matter © 2011 Elsevier B.V. All rights reserved.
doi:10.1016/j.molcata.2011.01.027

Transition metal Schiff base complexes have played for some time an important role in the oxidation of hydrocarbon feedstocks (olefins, alkanes and aromatics) to their respective oxygenated products. Herein, we report the immobilization of three cobalt Schiff base complexes onto SiO_2–Al_2O_3 mixed oxide, covalently bound through two typical linkers with different flexibility and spacer (3-aminopropyl and 2-aminoethyl-3-aminopropyl), and their remarkable catalytic activities and excellent selectivity in the catalytic oxidation of ethylbenzene in the liquid phase using *tert*-butyl hydroperoxide as the oxidant *without the need of any solvent* and reducing reagent.

The reason for choosing this particular mixed oxide was the properties such as low thermal expansion and conductivity, low dielectric constant, excellent creep resistance, robust chemical and thermal stability, good high temperature strength and oxidation resistance [13].

The synthesized materials were characterized by FT-IR spectroscopy, UV–Vis, CHN elemental analysis, ICP-MS, SEM, TEM, EPR, cyclic voltammetry (CV) and electrochemical impedance spectroscopy (EIS). Also, the influence of electrochemical potential and study of electrochemical behavior of the complex-immobilized materials on the catalytic activity of them was studied by electrochemical methods such as cyclic voltammetry (CV) and electrochemical impedance spectroscopy (EIS).

2. Experimental

2.1. Materials

All reagents (A.R.) were purchased from Merck or Fluka and were used without further purification, except that solvents were treated according to standard methods. Graphite powder (particle diameter = 0.1 mm) and carbon nanotubes [>90% MWCNT basis, $d \times l$ = (110–70 nm) × (5–9 μm) (Fluka)] were used as the substrates for the preparation of the carbon paste electrode as a working electrode (WE).

2.2. Characterization

Diffuse reflectance spectra were recorded on a JASCOV-550 UV–Vis spectrophotometer. Fourier transform IR spectra were measured using a JASCO FT/IR (680 plus) spectrometer. The spectra of solids were obtained using KBr pellets. The vibrational transition frequencies are reported in wave numbers (cm^{-1}). Elemental analysis was performed by a CHNO-Rapid Heraeus elemental analyzer (Wellesley MA). Chemical analyses were carried out by inductively coupled plasma optical emission spectroscopy (ICP-OES) using a Shimadzu ARL 34000 instrument (spectroflamed; typically, 30 mg sample was dissolved in 500 μL 40% HF solution, 4 mL 1:4 H_2SO_4:H_2O solution and 45 mL H_2O). Nitrogen (99.999%) adsorption experiments have been performed at 76 K using a volumetric apparatus (Quantachrome NOVA automated gas sorption analyzer). Before the adsorption experiments, the sample was outgassed at 393 K for 16 h. The specific surface areas are calculated from the BET method [14]. Transmission electron microscopy (TEM) was carried out on the powder samples with a Tecnai F30TEMoperating at an accelerating voltage of 300 kV. In addition, energy dispersive X-ray analysis was conducted on each sample. Electrochemical measurements were carried out with Micro-Autolab, ptentiostat/galvanostat instrument (μ3AUT70751), connected to a three-electrode cell. Conventional three electrodes cells were used for all experiments. The modified multi-walled carbon nanotubes paste electrode used as a working electrode, platinum wire as an auxiliary electrode, and an Ag/AgCl/KCl electrode as a reference electrode were used.

Electrochemical impedance measurements were carried out in a conventional three-electrode cell, powered by an electrochemical system comprising the Autolab (AUT83593) at a frequency range of 0.1–10,000 Hz. The AC voltage amplitude was 5 mV.

2.3. Reaction conditions

A typical procedure for the liquid-phase oxidation of ethylbenzene to acetophenone was as follows: 50 mg of the catalyst, 1.14 mL of ethylbenzene (2.0 mmol), 1.34 mL of 80% TBHP (2.0 mmol) and n-decane as internal standard were in turn introduced into a 50 mL one-neck flask equipped with a condenser. The flask was immersed in an oil bath in order to make the working temperature constant at 353 K for a predetermined time (24 h) with continuous stirring. The small aliquots of samples were withdrawn from the reaction flask at different time intervals with a HPLC syringe. The contents were centrifuged to separate the catalyst and the liquid layer was analyzed. Products were monitored by GC (Agilent technologies 6890N), HP-50 capillary column (30.0 m × 250 μm × 0.25 μm), FID detector, and high purity helium as carrier gas, and the products were identified by GC–MS (Shimadzu QP 5000; DB 1 column; 30 m × 0.25 mm): column temperature, 353 K; injection and detection port temperature, 523 K; and using a temperature program (the oven temperature held at 353 K for 1 min then raised from 353 K to 473 K at 15 K/min and held at 473 K for 3 min). Identification of products was done by comparing the GC retention times of expected products with those of standard samples. Leaching experiments were carried out in order to prove the heterogeneous character of the reactions. In representative tests, the catalyst was filtered out and the filtrate was analyzed for Co content using atomic absorption spectrophotometry (AAS).

2.4. Preparation of the organometallic functionalized SiO_2–Al_2O_3 mixed-oxide

SiO_2–Al_2O_3 mixed-oxide was prepared according to the procedure reported before [15]. The support is denoted as SiO_2–Al_2O_3 (1:1). The modified support (Scheme 1) was prepared by refluxing 5.2 g SiO_2–Al_2O_3 (activated at 823 K for 6 h under air) with 3.5 mL of 3-aminopropyl-trimethoxysilane (0.0195 mol) in dry dichloromethane (100 mL) for 24 h. The solid was filtered and washed off with methanol, dichloromethane and dried at 373 K under vacuum for 6 h. The same reaction condition was used for the functionalization of SiO_2–Al_2O_3 (1:1) with 2-aminoethyl-3-aminopropyl-trimethoxysilane. The functionalized SiO_2–Al_2O_3 (1:1) mixed oxides are identified hereafter by Si/Al-*pr*-NH_2 and Si/Al-*pr*-NH-*et*-NH_2. Then, aldehyde or ketone (salicylaldehyde, methyl-2-pyridylketone or pyridine-2-carbaldehyde) was added to a suspended solution of Si/Al-*pr*-NH_2 or Si/Al-*pr*-NH-*et*-NH_2, in dry methanol. The mixture was refluxed for 24 h to prepare a Schiff base (*vide* Scheme 1) on the surface of the mixed-oxide (a bi-dentate ligand).

Catalysts containing Co(III)–Schiff base complexes were obtained by stirring 0.5 g of the hybrid material, Si/Al mixed-oxide-Schiff base ligand, with Co $(OCOCH_3)_2$ $4H_2O$ (5.4 mmol), and LiCl (8.5 mmol) in 30 mL of ethanol at reflux for 24 h. Then, the resulting catalyst (brown powder) was filtered off, washed with copious of ethanol and methanol and dried in a vacuum at 60 °C.

2.5. Preparation of the electrode

10 mg of the immobilized Co catalyst onto the SiO_2–Al_2O_3 hand mixed with 79 mg of graphite powder and 10 mg of multi-wall carbon nanotubes in a mortar and pestle. Using a syringe, 0.88 g paraffin was added to the mixture and mixed well for 40 min until a uniformly wetted paste was obtained. The paste was then packed

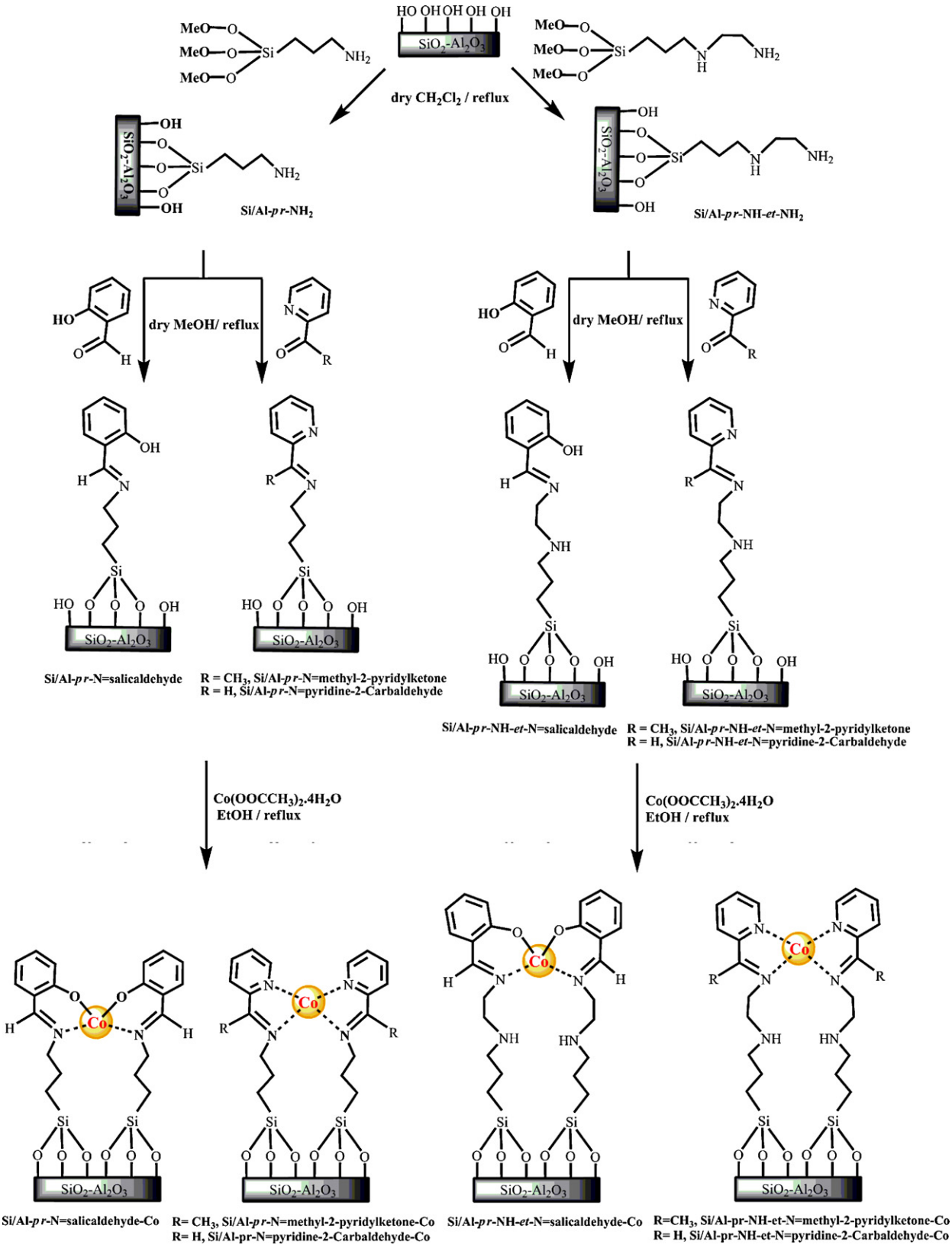

Scheme 1. Immobilization procedure of the immobilized Co(II)-Schiff base complexes onto the SiO_2–Al_2O_3 mixed-oxide.

into a glass tube. Electrical contact was made by pushing a copper wire down the glass tube into the back of the mixture. When necessary, a new surface was obtained by pushing an excess of the paste out of the tube and polishing it on a weighing paper.

2.6. Recommended procedure for electrochemical analysis

The blend of immobilized Co catalyst and multiwall carbon nanotubes paste electrode was polished with a white and clean filter

paper. To record of cyclic voltammograms for the immobilized Co catalyst onto the SiO_2–Al_2O_3, 10.0 mL of 0.1 M phosphate buffer at (pH 10.0), was transferred into an electrochemical cell. The initial and final potentials were adjusted to +0.00 and +1.00 V *versus* Ag/AgCl, respectively. The cyclic voltammograms were recorded with scan rate 100 mV s^{-1} to give the oxidation and reduction signals.

3. Results and discussion

The structures of the obtained organometallic-modified Si/Al mixed oxides were confirmed by elemental analysis, BET (N_2 adsorption–desorption technique), FTIR (Infrared spectroscopy serves as a main investigation tool), DR UV–Vis, ICP-MS, TEM, EPR, cyclic voltammetry (CV) and electrochemical impedance spectroscopy (EIS). Elemental analysis showed that the addition of salicylaldehyde, methyl-2-pyridylketone and pyridine-2-carbaldehyde to the surface amines was approximately stoichiometric.

In fact, during the preparation of the organometallic-modified Si/Al mixed oxides, the same amounts of alkoxysilane agents were deliberately introduced in the anchoring solution (moles of alkoxysilane agent/grams Si/Al mixed oxide = 3.7 mmol/g) to obtain the similar amounts of linkers on the surface of Si/Al mixed oxide. In addition, during the condensation and immobilization, the dosage of aldehyde (salicylaldehyde or pyridine-2-carbaldehyde) or ketone (methyl-2-pyridylketone) were excessive to minimize the amounts of the undesired residual linkers on the support. The immobilized Schiff base ligands readily reacts with $[Co(OCOCH_3)_2]$ in EtOH to give the heterogeneous complexes. A change in color of the resulted powders can also be visualized during the reactions (Scheme 1). Loading of the immobilized catalyst was estimated from the cobalt content determined by ICP-AES and the Schiff base ligand content determined by elemental analysis (Table 1). Moreover, the densities of cobalt complexes per surface area in all immobilized complexes were not similar, showing the almost non-identical condensation and coordination degrees of active moieties present in the complex-immobilized materials. On the other hand, the difference in catalyst loading could be due to the difference in ligands structure and linker too. The result is summarized in Table 1.

The textural properties of the samples, evaluated from the low temperature nitrogen adsorption revealed a decrease in the specific surface area (S_{BET}). The surface area decreased further on the modified support with 3-aminopropyl with the exception of saliclaldehyde. Pore diameters of all organometallic-modified Si/Al mixed oxides (Table 1) are similar in the range of 16–20 Å.

3.1. IR spectroscopy

Infrared wave numbers (cm^{-1}) of significant valence vibrations helpful for identification of the immobilized ligands and of complexes are collated in Table 2 and Fig. 1. The band at around 1050 cm^{-1} is due to the asymmetric stretching vibration of $(Si/Al)O_4$ units of Si/Al mixed oxide. The bands at 2943–2921 and 2877–2845 cm^{-1} are assigned to the stretching mode of $-CH_2$ groups. From the presence of these bands, it can be inferred that the Si/Al mixed oxide is modified by amine spacer groups successfully. The N–H deformation peak at 1540–1560 cm^{-1} confirms the successful functionalization of 3-APTES and 2-AE-3-APTMS on the Si/Al mixed oxide. In agreement with previously reported data [16,17], C=N (Schiff base) absorptions are in the 1639–1631-cm^{-1} range, the skeletal vibration of benzene in the 1600–1590 cm^{-1} range and the vibration of C=N in pyridine groups are in the 1571–1569 cm^{-1} range [18] (Table 2).

Table 1
Chemical composition and physicochemical properties of the immobilized Co–Schiff base-complex onto the SiO_2/Al_2O_3 mixed oxide.

Catalyst	Elemental analyses (wt%)[a]		Organic functional group (mmol/g mixed oxide)[b]	Immobilized Co–Schiff base-complex (mmol/g mixed oxide)[c]	% Coordinated Schiff base groups to Co[c]	Structural parameters[d]		
	N	Co				Surface area (m^2/g)	Pore volume (cm^3/g)	Pore diameter (Å)
SiO_2/Al_2O_3 mixed oxide	–	–	–	–	–	243	0.028	20
Si/Al-*pr*-N = salicylaldehyde-Co	3.2	2.5	2.3	0.42	36	94	0.019	15
Si/Al-*pr*-NH-*et*-N = salicylaldehyde-Co	4.9	3.2	3.5	0.54	61	104	0.021	17
Si/Al-*pr*-N = methyl-2-pyridylketone-Co	3.9	3.0	2.8	0.51	72	109	0.023	16
Si/Al-*pr*-NH-*et*-N = methyl-2-pyridylketone-Co	5.7	3.4	4.1	0.57	83	101	0.025	18
Si/Al-*pr*-N = pyridine-2-carbaldehyde-Co	4.0	2.6	2.9	0.44	60	114	0.023	17
Si/Al-*pr*-NH-*et*-N = pyridine-2-carbaldehyde-Co	4.6	2.9	3.3	0.49	89	94	0.020	16

[a] Nitrogen was estimated from the elemental analyses. Co content determined from ICP analysis.
[b] Determined from the N-contents.
[c] Determined from the Co-content, assume that cobalt ions coordinated with Schiff bases.
[d] The pore size calculated using the BJH method.

Table 2
Infrared attributions of significant vibrations for complexes.

System	FT-IR data (cm^{-1})						
	ν(C–H) aliphatic	ν(C–H) aromatic	ν(N–H)	ν(C=N)	ν(C=C)	Ring	ν(C–O)
Si/Al-*pr*-NH_2	2933, 2853	–	1560–1545	–	–	–	–
Si/Al-*pr*-NH-*et*-NH_2	2927, 2854	–	1560–1545	–	–	–	–
Si/Al-*pr*-N=salicylaldehyde	2925, 2854	3068, 3056	1560–1545	1633,	1540	1457, 760	1278
Si/Al-*pr*-NH-*et*-N = salicylaldehyde	2925, 2854	3068, 3056	1560–1545	1639,	1540	1457, 760	1278
Si/Al-*pr*-N=methyl-2-pyridylketone	2927, 2852	3066	1560–1545	1635,1571	1590,1434	1458	–
Si/Al-*pr*-NH-*et*-N=methyl-2-pyridylketone	2940, 2877	3069	1560–1540	1635	1591,1435	1455, 751	–
Si/Al-*pr*-N=pyridine-2-carbaldehyde	2925, 2852	3064, 3052	1560–1550	1633, 1569	1540,1591, 1437	1457, 750	–
Si/Al-*pr*-NH-*et*-N=pyridine-2-carbaldehyde	2931, 2856	3054	1560–1540	1631 1569	1590, 1435	1469, 752	–
Si/Al-*pr*-N=salicylaldehyde-Co	2930, 2855	3057, 3013	1560–1545	1644,	1535,	1440	1280
Si/Al-*pr*-NH-*et*-N = salicylaldehyde-Co	2924, 2855	3065	1560–1545	1642,	1538	1453,	1310
Si/Al-*pr*-N=methyl-2-pyridylketone-Co	2929, 2853	3065	1560–1545	1640, 1568	1542, 1535	1473	–
Si/Al-*pr*-NH-*et*-N=methyl-2-pyridylketone-Co	2928, 2856	3061, 3013	1560–1545	1640, 1568	1540, 1535,1436	1457, 1473	–
Si/Al-*pr*-N=pyridine-2-carbaldehyde-Co	2927, 2855	3058	1560–1545	1638, 1571	1542, 1438	1470	–
Si/Al-*pr*-NH-*et*-N=pyridine-2-carbaldehyde-Co	2960, 2923,2851	3058	1555–1540	1639, 1569	1544, 1535,1439	1465	–

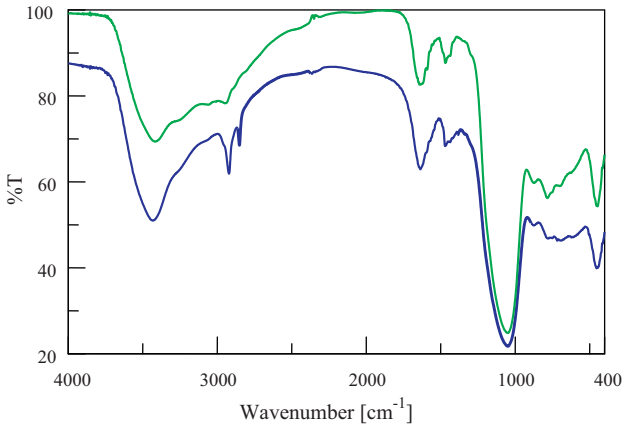

Fig. 1. FT-IR spectra of organo-functionalized SiO_2–Al_2O_3 mixed-oxide and immobilized cobalt nanoparticles. Expanded FT-IR spectra of: (above insert) Si/Al-*pr*-NH-*et*-N = methyl-2-pyridylketone-Co (bottom insert) Si/Al-*pr*-NH-*et*-N = methyl-2-pyridylketone.

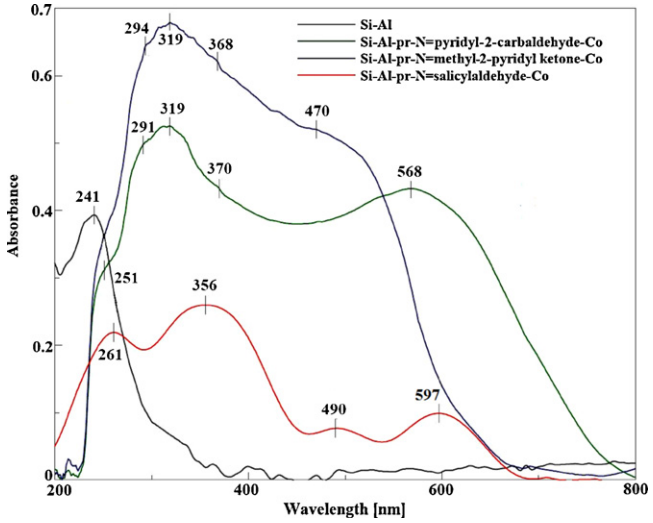

Fig. 2. UV–Vis diffuse reflectance spectra of the immobilized Co(II)-Schiff base complexes onto the SiO_2-Al_2O_3 mixed-oxide modified with 3-aminopropyl-trimethoxysilane.

The peaks in the 3070–3052 cm^{-1} range are attributed to the C–H stretching vibrations of phenyl group. The FT-IR spectra of all Schiff base systems clearly show the C–H vibration of Ph and Py group at 3070–3052 cm^{-1}, which further confirming the existence of phenyl and pyridine groups on the Si/Al mixed oxide after the immobilization of the ligands. The modes of metal coordination with the two N and O donor ligands through the phenolic oxygen and azomethine nitrogen of Schiff bases are evidenced from the blue shift (*ca.* 32 cm^{-1}) of ν(C–O) and the red shift (*ca.* 3–11 cm^{-1}) of the ν(C=N) vibrations with respect to the free ligand (Table 2). The FT-IR results demonstrate the formation of the Co(II) complexes immobilized on the Si/Al mixed oxide through 3-APTES and 2-AE-3-APTMS linkers.

3.2. DR UV–Vis spectroscopy

To gain insight into the effect of Si/Al mixed oxide modifying with Co(II)–Schiff base-complexes, the UV–Vis diffuse reflectance spectra of the synthesized heterogeneous materials were recorded at room temperature in the range of 230–800 nm. The UV–Vis spectra of the Si/Al mixed oxides and different immobilized Co(II) complexes are shown in Figs. 2 and 3. The UV–Vis spectrum of the Si/Al mixed oxide only had a side-band adsorption near 244 nm, while the spectra of the immobilized Co(II) complexes were dominated by strong absorptions in the 230–370 nm due to the $\pi \rightarrow \pi^*$ and $n \rightarrow \pi^*$ transitions of the phenyl, pyridine and C=N groups. Furthermore, the Co(II)-complexes exhibited the observed

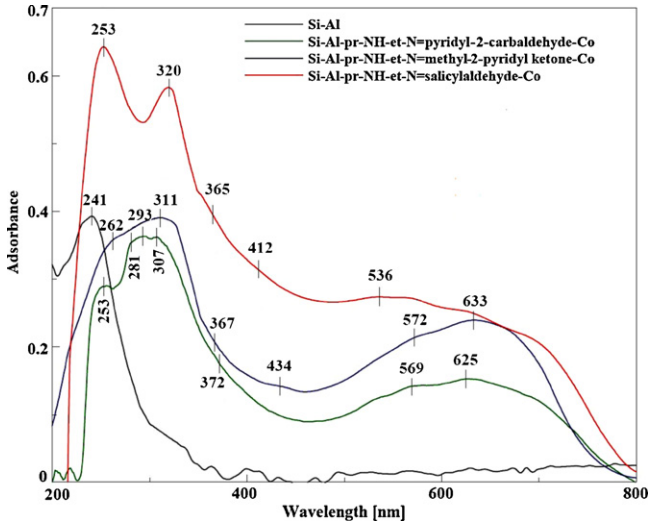

Fig. 3. UV–Vis diffuse reflectance spectra of the immobilized Co(II)-Schiff base complexes onto the SiO_2–Al_2O_3 mixed-oxide modified with 2-aminoethyl-3-aminopropyl-trimethoxysilane.

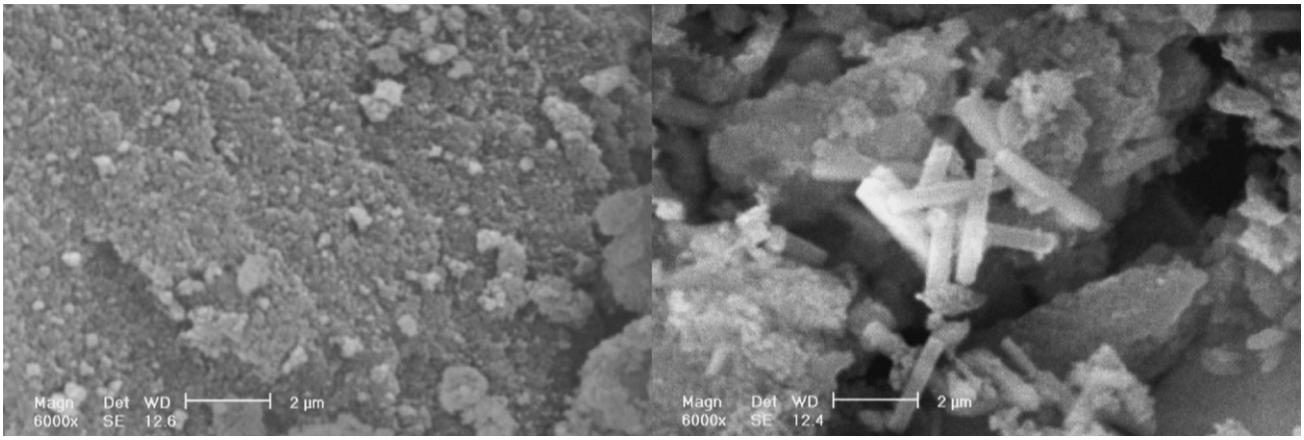

Fig. 4. SEM micrographs of SiO_2–Al_2O_3 mixed-oxide (left) and Si/Al-pr-NH-et-N = methyl-2 pyridylketone-Co (right).

shoulder around 390 and 490 nm, probably attributable to the ligand-to-metal charge transfer of the $d \rightarrow \pi^*$ transitions, similar to metallosalen compounds [19,20]. Several low intensity asymmetric shoulder broad bands appeared over 500 nm in the visible region at λ = 500–650 nm are attributed to the $d \rightarrow d$ transitions expected for the cobalt complexes with a square pyramidal geometry, ($d_{xz} \rightarrow d_{x^2-y^2}$), ($d_{yz}$, $d_{xy} \rightarrow d_{x^2-y^2}$) and ($d_{z^2} \rightarrow d_{x^2-y^2}$) (decreasing energy), which were similar to related metal (salen) compounds described in the literatures [21–23]. The UV–Vis spectra of the heterogenized catalysts revealing that the organocobalt complexes were immobilized by chemical bonds over the Si/Al mixed oxide structure and also confirmed the coordination of the ligands to the central metallic ion.

Consequently, DRUV–Vis and FT-IR spectra expose that the immobilized Co–Schiff base ligands are synthesized upon coordination to the organo-functional groups. The charge transfer bands (Figs. 2 and 3), the stretching frequency at 1630–1645 cm^{-1} (Table 2), elemental analyses (Table 1) and thermal analyses (data not published) clearly confirm that the Schiff base ligand and C=N groups are not affected or destroyed through immobilization on the functionalized Si/Al mixed oxide.

3.3. SEM and TEM images

SEM images of the parent SiO_2–Al_2O_3 mixed-oxide and the Si/Al-*pr*-NH-*et*-N = methyl-2-pyridylketone-Co sample are shown in Fig. 4. The surface modification has changed the morphology of the surface. The images show that the organic modifier has increased the porosity of the surface.

The TEM micrographs and size distributions (100 and 50 nm) of the nanoparticles are shown in Fig. 5, respectively. TEM images indicated that the most of the prepared nanoparticles are spherical shaped and have size less than 70 nm.

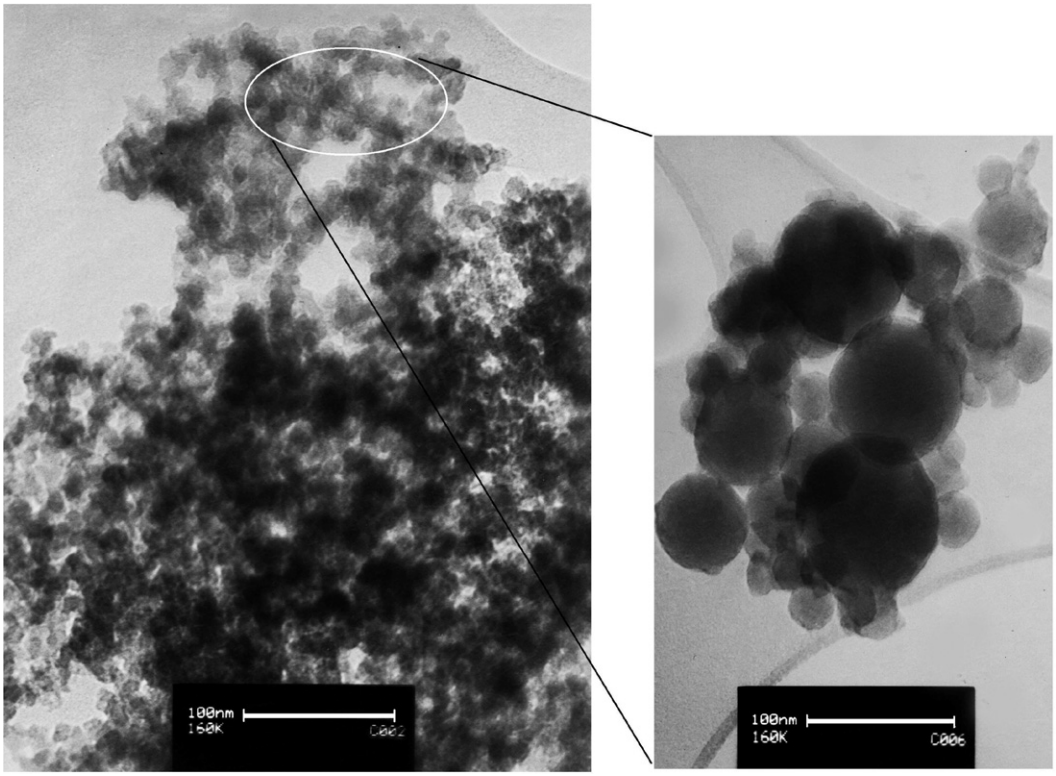

Fig. 5. Co nanoprticles: TEM micrographs of Si/Al-*pr*-NH-*et*-N = methyl-2-pyridylketone-Co.

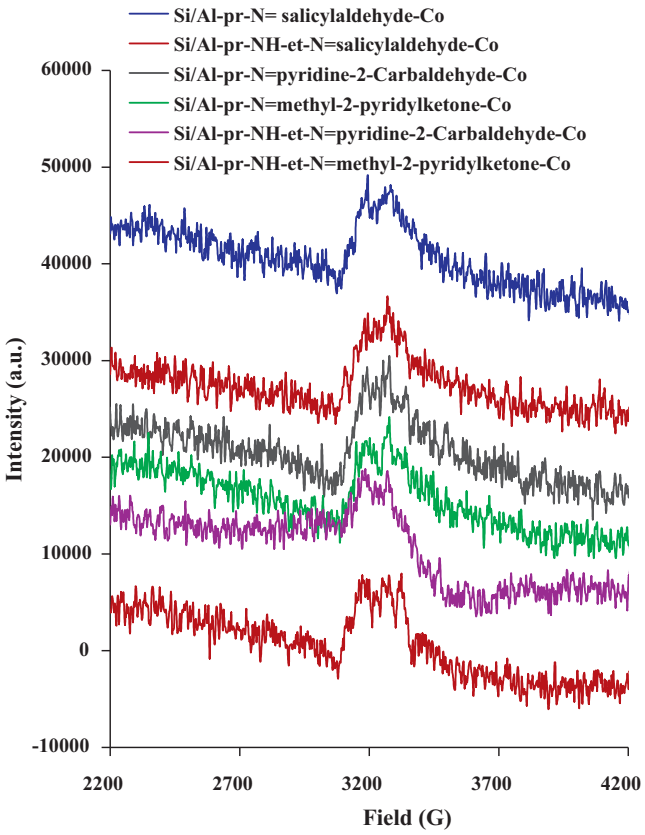

Fig. 6. EPR spectra of of the immobilized Co(II)-Schiff base complexes onto the SiO_2–Al_2O_3 mixed-oxide.

3.4. EPR spectroscopy

EPR spectroscopy has been employed to confirm on the oxidation states and the chemical environment of Co species present in our samples. The X-band EPR spectra of the immobilized Co–Schiff base-complexes measured at room temperature are depicted in Fig. 6.

The appearance of these EPR signals, characteristic of Co(II), indicates that, part of the Co ions are presented in from the +2 oxidation state upon immobilization on the functionalized SiO_2/Al_2O_3 mixed oxide. The ESR spectra all appear to have a very broad line and the most prominent is a broad feature centered around $g = 1.95$, with the wide wings. In fact, the peak broadening and wings are due to dipole–dipole interactions [24], and they are predominant in the spectra of higher loaded samples (samples containing more than 1.5 wt% Co)[25].

Microcrystalline nanoparticles often yield characteristic EPR spectra with features distinctly different from those observed for magnetically isolated ions [26]. The detailed features of the resonances depend strongly on shape and size distributions and on the magnetic properties of the particles. Consequently, with regard to the EPR spectra and TEM photo, the broad features around $g_{av} = 2.05$ are probably characteristic of superparamagnetic relaxation as it concerned with the magnetic moment of the whole particles and either may be due to the highly dispersed nanoparticle of Co species (Fig. 6).

3.5. Catalytic performance

The performance of the Co nanocatalysts was tested in ethylbenzene oxidation *without the need of any solvent* and reducing reagent at 353 K. The best oxidant was t-butyl hydroperoxide

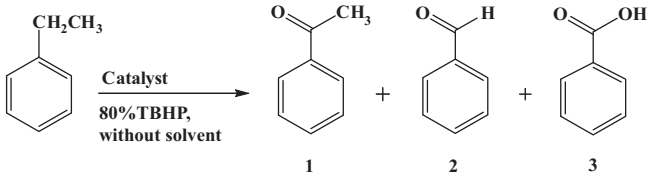

Scheme 2. Formation of the products over Co nanocatalysts.

80% (TBHP), because aqueous hydrogen peroxide (H_2O_2) did not show any reactivity in this reaction. The results of the % selectivity to acetophenone and % conversion of ethylbenzene with the reaction time are presented in Table 3. The conversion and selectivity were monitored by GC analysis. Products were identified by considering their GC–MS and by comparison with the GC of the authentic samples. The oxidation takes place on the α-carbon of the alkylbenzene. Formation of the products acetophenone, 1, benzaldehyde, 2, and benzoic acid, 3, are illustrated in Scheme 2. It is remarkable to mention that no oxidation was observed in the aromatic ring of the ethylbenzene. The catalytic activity of the solid catalysts was higher in solvent free condition than in the presence solvent such as CH_3CN (data not shown). The decrease in conversion under solvent conditions is attributed to the blocking of active sites by solvent molecules or may be explained by the diffusion competition of the solvent and the substrate [27]. Generally, acetophenone was found to be the main product, along with minor quantities of benzaldehyde and benzoic acid. In fact, acetophenone selectivity was initially increased gradually (on Si/Al-*pr*-NH-*et*-N = methyl-2-pyridylketone-Co, Si/Al-*pr*-N = salicylaldehyde-Co, Si/Al-*pr*-N = methyl-2-pyridylketone-Co and Si/Al-*pr*-NH-*et*-N = salicylaldehyde-Co) and on some catalysts sharply (Si/Al-*pr*-NH-*et*-N = pyridine-2-carbaldehyde-Co and Si/Al-*pr*-N = pyridine-2-carbaldehyde-Co) from 2 to 12 h. This indicates that the side reactions become less plausible with the progress of the reaction leading to increases in the selectivity to acetophenone and decreases in the selectivity to benzaldehyde and benzoic acid. After 12 h, the acetophenone selectivity was more or less constant up to 24 h and probably inhibits the side reactions and therefore the selectivity of acetophenone did not change. The formation of other products viz. benzaldehyde may arise from the cleavage of the C–C bond while the presence of benzoic acid may result from the oxidation of benzaldehyde.

As presented in Table 3, the selectivity over different immobilized Co-complexes after 24 h changed in the following order: Si/Al-*pr*-NH-*et*-N = methyl-2-pyridylketone-Co (99%) > Si/Al-*pr*-NH-*et*-N = pyridine-2-carbaldehyde-Co (85%) > Si/Al-*pr*-NH-*et*-N = salicylaldehyde-Co (78%) > Si/Al-*pr*-N = salicylaldehyde-Co (75%) > Si/Al-*pr*-N = pyridine-2-carbaldehyde-Co (67%) > Si/Al-*pr*-N = methyl-2-pyridylketone-Co (63%). Probably, the electronic effects of the ligands may change the selectivity to acetophenone. As a result, high selectivity to acetophenone was achieved using catalysts with pyridine groups instead of phenyl groups in the ligand structure. The most effective system in terms of selectivity was Si/Al-*pr*-NH-*et*-N = methyl-2-pyridylketone-Co, where the backbone of the catalyst was modified with 2-AE-3-APTMS.

Ethylbenzene conversion and catalytic activity (turnover) were monitored after 2 h of the reaction and was increased gradually up to 24 h (Table 3). The reaction was almost complete after about 24 h, when the TBHP efficiency reaches a maximum. Majority of the prepared catalysts were highly reactive and selective for the oxidation of ethylbenzene. As shown in Table 3 and Fig. 7, the catalyst, Si/Al-*pr*-NH-*et*-N = methyl-2-pyridylketone-Co, showed the most desired catalytic performances (86%), that could be due to the cobalt content of the catalyst (0.57 mmol g^{-1}). The EB conversion after 24 h over different catalysts follows

Table 3
Oxidation of ethylbenzene: variation with reaction time over different cobalt nanocatalysts.[a]

Catalyst	Time (h)	Conversion (mol%)	TON[b]	Selectivity (mol%) (acetophenone)
Si/Al-*pr*-N = salicylaldehyde-Co	2	20.0	19.0	60.0
	6	32.8	–	65.1
	12	37.8	–	68.0
	18	40.0	–	74.0
	24	43.8	41.6	75.2
Si/Al-*pr*-NH-*et*-N = salicylaldehyde-Co	2	25.3	18.6	60.1
	6	37.6	–	66.8
	12	46.4	–	73.5
	18	57.3	–	76.9
	24	59.6	43.7	78.2
Si/Al-*pr*-N = pyridine-2-carbaldehyde-Co	2	16.8	15.2	37.9
	6	24.1	–	51.1
	12	40.2	–	59.7
	18	47.4	–	65.9
	24	48.5	43.8	67.7
Si/Al-*pr*-NH-*et*-N = pyridine-2-carbaldehyde-Co	2	24.0	19.8	53.0
	6	41.8	–	66.8
	12	57.6	–	73.5
	18	68.0	–	80.0
	24	77.3	63.8	85.8
Si/Al-*pr*-N = methyl-2-pyridylketone-Co	2	21.4	17.0	47.1
	6	31.0	–	50.3
	12	47.0	–	58.5
	18	52.0	–	61.0
	24	55.7	44.1	63.1
Si/Al-*pr*-NH-*et*-N = methyl-2-pyridylketone-Co	2	24.6	17.4	78.7
	6	43.1	–	81.3
	12	58.4	–	87.1
	18	76.9	–	95.0
	24	86.8	61.4	99.9

[a] Reaction condition: substrate (ethyl benzene) = 2.0 mmol, TBHP = 2.0 mmol, weight of the catalyst = 50 mg, T = 353 K.
[b] TON, turn over number, moles of substrate converted per mole of metal.

the order of: Si/Al-*pr*-NH-*et*-N = methyl-2-pyridylketone-Co (86%) > Si/Al-*pr*-NH-*et*-N = pyridine-2-carbaldehyde-Co (77%) > Si/Al-*pr*-NH-*et*-N = salicylaldehyde-Co (59%) > Si/Al-*pr*-N = methyl-2-pyridylketone-Co (55%) > Si/Al-*pr*-N = pyridine-2-carbaldehyde-Co (48%) > Si/Al-*pr*-N = salicylaldehyde-Co (43%). The Si/Al-*pr*-N = salicylaldehyde-Co catalyst showed the lowest conversion among the studied systems (43%). The poor reactivity of the last catalyst was probably related to the low cobalt content of this sample (0.42 mmol g^{-1} from ICP results).

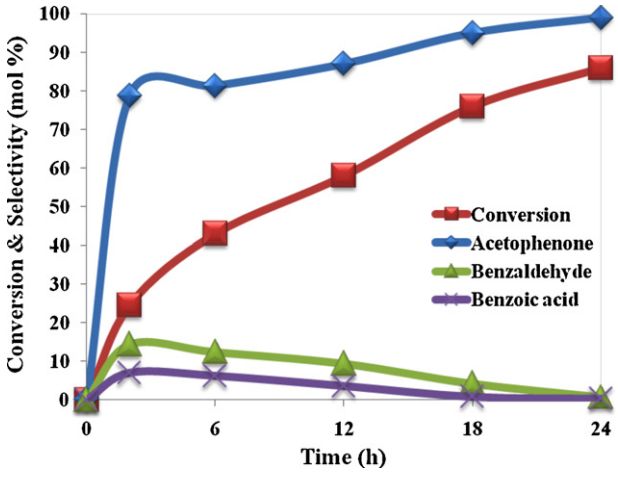

Fig. 7. Product distribution and catalytic activity *versus* time in the oxidation of ethylbenzene with TBHP catalysed by Si/Al-*pr*-NH-*et*-N = methyl-2-pyridylketone-Co at 353 K.

With regard to the obtained results, ethylbenzene oxidation activity of different immobilized Co-complexes over modified Si/Al mixed-oxide prepared with three different Schiff base ligands by the condensation between methyl-2-pyridylketone, pyridine-2-carbaldehyde and salicylaldehyde with two different amine linkers, 3-APTES and 2-AE-3-APTMS, varied significantly depending on their structures.

When comparison was made between the two catalysts prepared on 3-APTES and 2-AE-3-APTMS, significant differences are detected: the selectivity toward acetophenone as well as the activities was not the same for both systems. Among these, the catalyst prepared with 2-AE-3-APTMS showed the best performance compared with those synthesized with 3-APTES. Thus, as a competent statement, the conversion and selectivity of Co(II)–Schiff base-complexes on the modified Si/Al mixed oxide through 2-AE-3-APTMS were higher than those on 3-APTES. This difference apparently results from the different surface properties of the modified Si/Al mixed oxide with two spacers. When 3-APTES is the spacer, the steric hindrance and accessibility issues that caused by the surrounding alkyl chains at the catalytic site, leading to a significant decrease in the selectivity and reactivity (this point of view will be more discussed in Section 3.6). On the other hand, the increase in conversion and selectivity may be attributed to the improved surface hydrophobicity of modified Si/Al mixed oxide with 2-AE-3-APTMS and the reduced steric interaction of the immobilized Co-complexes with host support (mimicking homogeneous conditions) and also has increased the mobility of them (Keeping in mind that 2-AE-3-APTMS has a longer carbon chain than 3-APTES, and certainly enlarges accessibility issues of the catalytic sites to the substrate).

Besides coordination to a Schiff base ligand, the cobalt may also interact with the surface Si–OH and Al–OH groups of the Si/Al

Table 4
Effect of temperature on the oxidation of ethylbenzene with TBHP over Si/Al-*pr*-NH-*et*-N = methyl-2-pyridylketone-Co.

Time (h)	Conversion %		Selectivity %	
	323 K	353 K	323 K	353 K
2	19	24	67	79
6	32	43	75	81
12	47	58	85	87
18	64	76	91	95
24	76	86	95	99

mixed oxide structure. Thus, the materials of blank Si/Al mixed oxide that adsorbed cobalt were also used for oxidation experiment. It turned out that the conversion of ethylbenzene was almost 0%. Therefore, in the oxidation of ethylbenzene with TBHP, the possibility of absorbed cobalt onto the Si–OH and Al–OH groups bestow no contribution. The above observations suggest that the oxidations occur due to the catalytic nature of the chemically immobilized Schiff base complexes. Clearly, the Si/Al-*pr*-NH-*et*-N = methyl-2-pyridylketone-Co catalyst was vastly more selective to acetophenone (99%) and high active catalyst for oxidation of ethylbenzene to acetophenone (86%), therefore the rest of research was devoted on this catalyst.

Si/Al-*pr*-NH-*et*-N = methyl-2-pyridylketone-Co, the promising catalyst from the screening test, was further evaluated for catalytic activity for the oxidation of ethylbenzene with TBHP at 323 and 353 K, and the results are given in Table 4. It has been shown that the conversion and selectivity enlarged significantly with increasing temperature from 50 to 80 °C.

It must be emphasized that a successful complex immobilization must involve not only the efficiency of the immobilization strategy, but also the stability of the resulting material (support and complex) under the experimental catalytic reaction conditions. Consequently, to confirm the true heterogeneous nature of immobilized Co-complexes in ethylbenzene oxidation reactions with TBHP, the Si/Al-*pr*-NH-*et*-N = methyl-2-pyridylketone-Co catalyst was reused in the ethylbenzene oxidation several times. This catalyst was reused after the solid was separated from the liquid reaction mixture by centrifugation and followed by several washes. The results are presented in Fig. 8. Comparing the result in Fig. 8, shows that the selectivity of the reused catalyst remained almost unchanged after fourth cycles, but the catalytic reactivity (Fig. 8) fell gradually (in the fourth cycle, the conversion was only 61%, and about 25% reduction of conversion took place after 24 h). This could be due to the loss of the catalyst during filtration and washing. The AAS analysis indicates that the activity reduction was not mainly attributed to the leaching of cobalt during the catalytic runs because the AAS analysis of the reaction solutions after 24 h showed no leaching of cobalt, confirming that immobilized Co-complexes on the modified SiO_2–Al_2O_3 mixed-oxide have high stability during the catalytic process. Based on a reduced activity of the catalyst

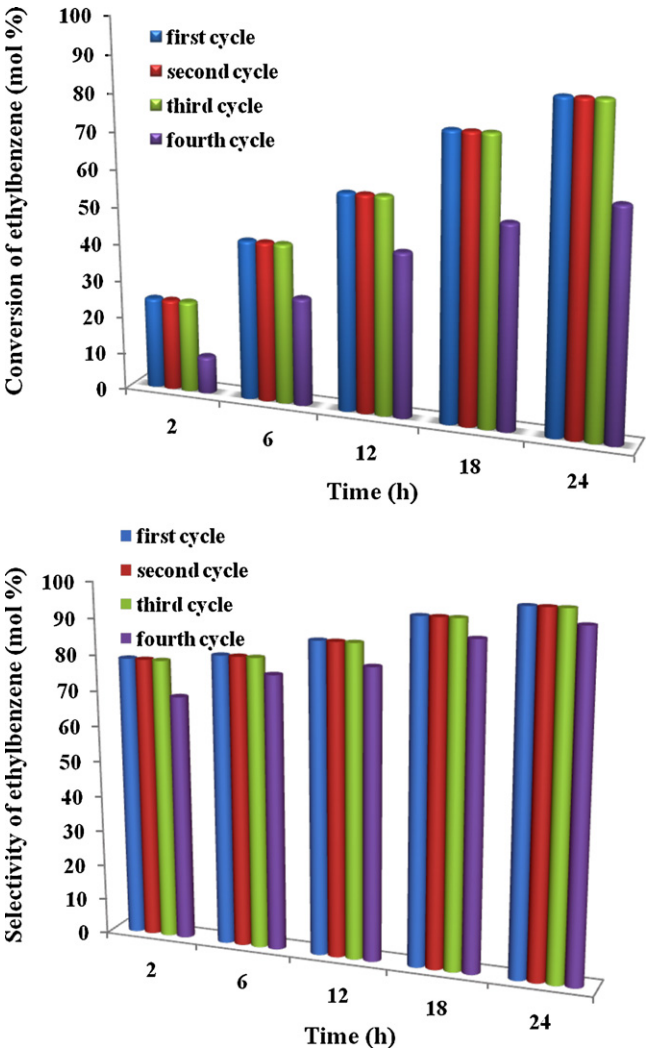

Fig. 8. Influence of the number of uses on the catalytic activity (above figure) and selectivity (lower figure) of Si/Al-pr-NH-et-N = methyl-2-pyridylketone-Co for oxidation of ethylbenzene to acetophenone under solventless condition at 353 K.

after last run, the authors conclude, that probably most of the catalytic activity has to be attributed to heterogeneous catalysis, and the leached metal should deposited on the surface of the support without playing any active role in the oxidation reaction. To further confirm that the reaction was catalysed by the heterogeneous catalyst, we added extra ethylbenzene to the filtrate after the removal of the catalyst and continued the reaction under the same conditions; the GC analysis showed that no more oxygenated products were produced.

Table 5
Comparison of figure of merit of the present work with other studies in the literature.

Catalyst (amount)[a]	Oxidant[b]	Reaction time (h)	*T* (K)/solvent	Ethylbenzene conversion (%)	Selectivity (%)[c]			
					AP	BZ	Other products	Ref.
CoTPP–P(4VP-co-St)/SiO (0.09 g)	O_2	0.2	368/–	24	98	–	2	[18]
Cobalt(III) complexe (2 mmol)	O_2	4	423/–	70.4	90.2	0.7	9.1	[8]
Co/MCM-41(0.05 g)	TBHP	24	353/–	26.8	85.0	9.1	5.9	[10]
$Co(OAc)_2$–SiO_2 (0.005 g)	TBHP	24	363/isooctane	65	100	–	–	[28]
Si/Al-*pr*-NH-*et*-N = methyl-2-pyridylketone-Co (0.05 g)	TBHP	2	353/–	24	79	14	7	This work
Si/Al-*pr*-NH-*et*-N = methyl-2-pyridylketone-Co (0.05 g)	TBHP	24	353/–	86	99	–	1	This work

[a] CoTPP–P(4VP-co-St)/SiO: Co tetraphenylporphyrins on P(4VP-co-St)/SiO_2.
[b] TBHP, *tert*-butyl hydroperoxide.
[c] AP, acetophenone; BZ, benzaldehyde.

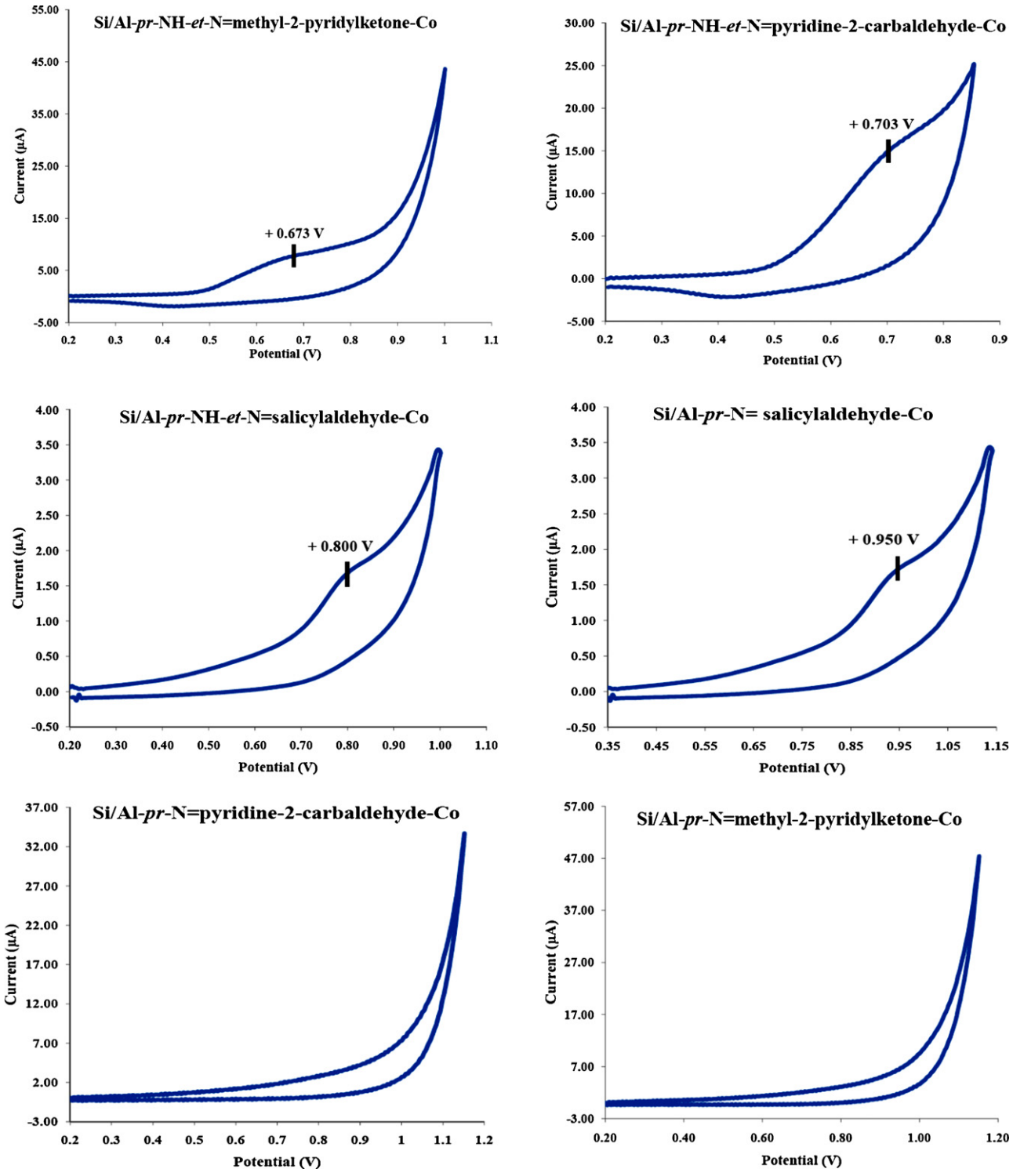

Fig. 9. Cyclic voltammograms of the different immobilized Co(II)-Schiff base complexes onto the SiO_2/Al_2O_3 mixed oxide through two linker at surface of multi walled carbon nanotube paste electrode.

Table 5 compares the catalysts used in the present study and the other catalysts used for oxidation of ethylbenzene, under different environmental conditions reported in the pertaining literature. When the ethylbenzene conversion (86%) and selectivity to acetophenone (99%) obtained in this study are compared with those published in the literature it can be observed that the catalyst employed here behave in an outstanding way.

3.6. Electrochemical study

As a follow up of this study, herein we have reported the study on electrochemical behavior of the immobilized Co(II)–Schiff base complexes onto the SiO_2–Al_2O_3 mixed-oxide. In this section, we describe application of electrochemical methods such as cyclic voltammetry CV and EIS to study the electrochemical behavior of the synthesized catalysts and comparing the dependence of the cat-

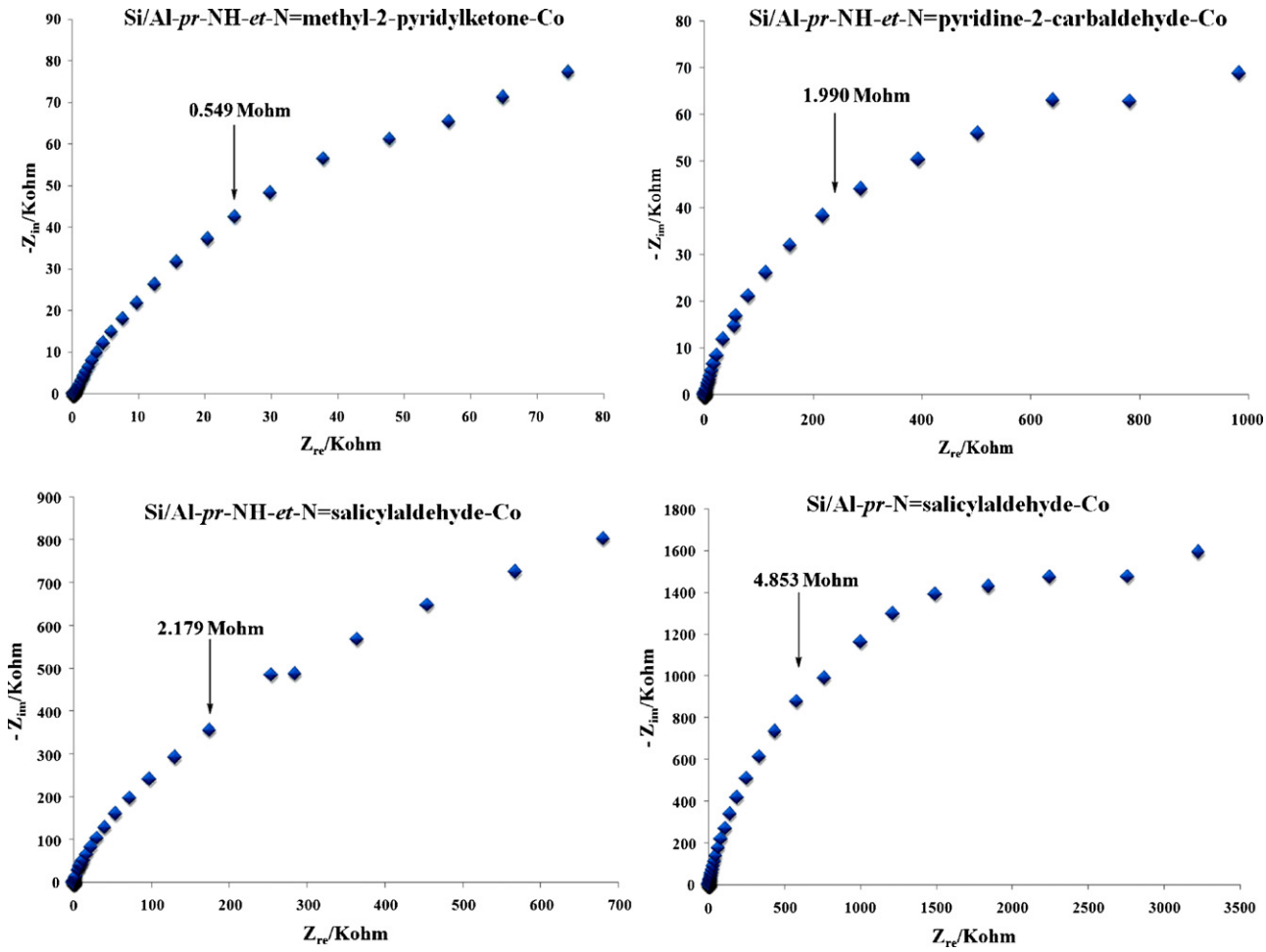

Fig. 10. Nyquist diagrams of the imaginary impedance (Z_{im}) *versus* the real impedance (Z_{re}) of the EIS obtained at the multi walled carbon nanotube electrode recorded for the different immobilized Co(II)-Schiff base complexes onto the SiO_2/Al_2O_3 mixed oxide through two linker.

alytic effect of the immobilized Co(II)–Schiff base complexes with their electrochemical behaviors. To our knowledge, there may be a few reports [13] that have used the electrochemical study of this type to demonstrate the reactivity of a catalyst by EIS technique with carbon paste and especially multi walled carbon nanotube paste electrodes.

Fig. 9 shows cyclic voltammograms obtained from different Co(II)-complexes in 0.1 M phosphate buffer solution (PBS) at (pH 10.0). The cyclic voltammograms exhibits an anodic peaks (E_{pa}) and corresponding cathodic peaks (E_{pc}) (with low intensity) *versus* $Ag|AgCl|KCl_{sat}$ (as a reference electrode) related to the Co^{3+}/Co^{2+} redox couple with quasi reversible behavior. The shift in the oxidation potential over different immobilized Co-complexes from low potential to high potential increased in the following order: Si/Al-*pr*-NH-*et*-N = methyl-2-pyridylketone-Co (E_{pa} = 0.673) < Si/Al-*pr*-NH-*et*-N = pyridine-2-carbaldehyde-Co (E_{pa} = 0.703) < Si/Al-*pr*-NH-*et*-N = salicylaldehyde-Co (E_{pa} = 0.800) < Si/Al-*pr*-N = salicylaldehyde-Co (E_{pa} = 0.950). As it is observed from Fig. 9, the Si/Al-pr-N = pyridine-2-carbaldehyde-Co and Si/Al-pr-N = methyl-2-pyridylketone-Co complexes did not show any oxidation peak at a surface of multi walled carbon nanotube paste electrode, probably, because the oxidation of those complexes occur after the solvent oxidation wall, that is, the oxidation peak was not observed. The electrochemical data about the oxidation correlate well with the selectivity and conversion data of the catalysts (*vide* Fig. 7). Moreover, the electrochemical measurements indicate that the oxidation of cobalt was easier and took place at lower potentials when the Co-complexes anchored on the modified SiO_2–Al_2O_3 mixed-oxide by 2-AE-3-APTMS than 3-APTES. As further discussed, the voltammograms of the modified SiO_2–Al_2O_3 mixed-oxide by 2-AE-3-APTMS indicate an easily oxidizable environment, in close agreement with the catalytic test (selectivity to acetophenone and conversion of ethylbenzene). The results show that anodic peak oxidation for the Si/Al-*pr*-NH-*et*-N = methyl-2-pyridylketone-Co has lower potential than the rest of complexes, this again being in agreement with the selectivity and conversion data of the catalysts (lower oxidation potential leads to the higher activity).

EIS was also employed to investigate the oxidation ability of the complexes at a surface of multi wall carbon nanotube paste electrode (MWCNTPE) as a powerful electrochemical technique in characterization and determination of kinetic parameters such as charge transfer resistance (R_{ct}) of the immobilized complexes and solution resistance (R_s). Fig. 10 presents Nyquist diagrams of the imaginary impedance (Z_{im}) *versus* the real impedance (Z_{re}) of the EIS obtained at the MWCNTPE recorded at 0.62 V dc-offset in the presence of immobilized Co(II)–Schiff base complexes onto the SiO_2–Al_2O_3 mixed-oxide in 0.1 mol L^{-1} PBS (pH 10.0). In the presence of the Co(II)-complexes, the Nyquist diagram comprises a depressed semicircle at high frequencies which may be related to the combination of charge transfer resistance for electro oxidation of these compounds and the double-layer capacitance (C_d), is generally a function of potential. The equivalent circuit compatible with the Nyquist diagram recorded is depicted in Scheme 3. In this

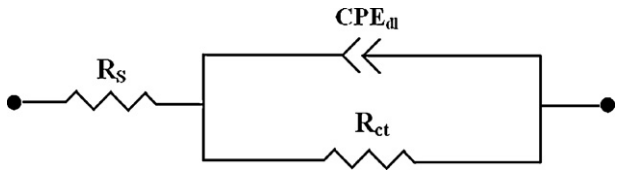

Scheme 3. The equivalent circuit compatible with the Nyquist diagram recorded.

circuit, R_s, CPE, and R_{ct} represent solution resistance, a constant phase element corresponding to the double-layer capacitance, and the charge transfer resistance associated with the oxidation of low-valence Co(II)-complexes species, respectively. The result shows that in the presence of different Co(II)-complexes the value of R_{ct} was altered. The value of charge transfer resistance is equal to the ability of a compound for participation in electrooxidation reaction [29]. Furthermore, in the mentioned circuits, the charge-transfer resistance of the electrode reaction is the only circuit element that has a simple physical meaning describing how fast the rate of charge transfer during electro-oxidation of the Co(II)–Schiff base-complexes changes with the electrode potential. Consequently, each compound that has high charge transfer resistance is inferior due to the inefficiency of the compound in oxidation of reactant to the desired product. Therefore, we determined the value of this parameter (R_{ct}) for Co(II) complexes used in this study, and comprehending the activity of these complexes in oxidation reaction. The charge transfer resistance of different catalysts follows the order Si/Al-*pr*-NH-*et*-N = methyl-2-pyridylketone-Co (R_{ct} = 0.549 Mohm) < Si/Al-*pr*-NH-*et*-N = pyridine-2-carbaldehyde-Co (R_{ct} = 1.990 MΩ) < Si/Al-*pr*-NH-*et*-N = salicylaldehyde-Co (R_{ct} = 2.179MKΩ) < Si/Al-*pr*-N = salicylaldehyde-Co (R_{ct} = 4.853 MΩ) (*vide* Table 1S). Noticeably, with regard to the cyclic voltammograms data we could not obtained any R_{ct} for Si/Al-*pr*-N = pyridine-2-carbaldehyde-Co and Si/Al-*pr*-N = methyl-2-pyridylketone-Co complexes (may be due to the oxidation of the considered complexes after the solvent oxidation wall). Therefore, this is certainly obvious that these complexes have a high R_{ct} rather than the other complexes. In view of the above observations, that is, the diminishing in the charge transfer resistance and influence of the charge transfer resistance on the selectivity and conversion of the catalysts, we consider that the immobilized Co-complexes on the modified Si/Al mixed oxide through 2-AE-3-APTMS indicate a lower R_{ct} than 3-APTES, probably, due to raised the mobility of them (2-AE-3-APTMS has a longer carbon chain than 3-APTES and might make the catalytic sites more accessible to the substrate) and decreased their interaction with the Si/Al mixed oxide support. Thus, it leads to the decreasing of R_{ct} and increasing the ability of the catalysts for presence and partnership in electrooxidation reaction.

This was very interesting that the results of selective oxidation efficiency of immobilized Co(II)–Schiff base complexes on SiO_2–Al_2O_3 mixed-oxide in the oxidation of ethylbenzene to acetophenone with TBHP, have close compatibility and correlation with observations of the E_{pa} and charge transfer resistance (R_{ct}) that obtained by cyclic voltammetry and EIS methods, respectively.

As further discussed, the oxidation potential of the Si/Al-*pr*-NH-*et*-N = methyl-2-pyridylketone-Co was lower than the other catalysts (Fig. 9). Also, in EIS, the Si/Al-*pr*-NH-*et*-N = methyl-2-pyridylketone-Co has lower charge transfer resistance than the other complexes (Fig. 10). Therefore, with regard to the above consideration, the catalyst could better associate in oxidation reaction

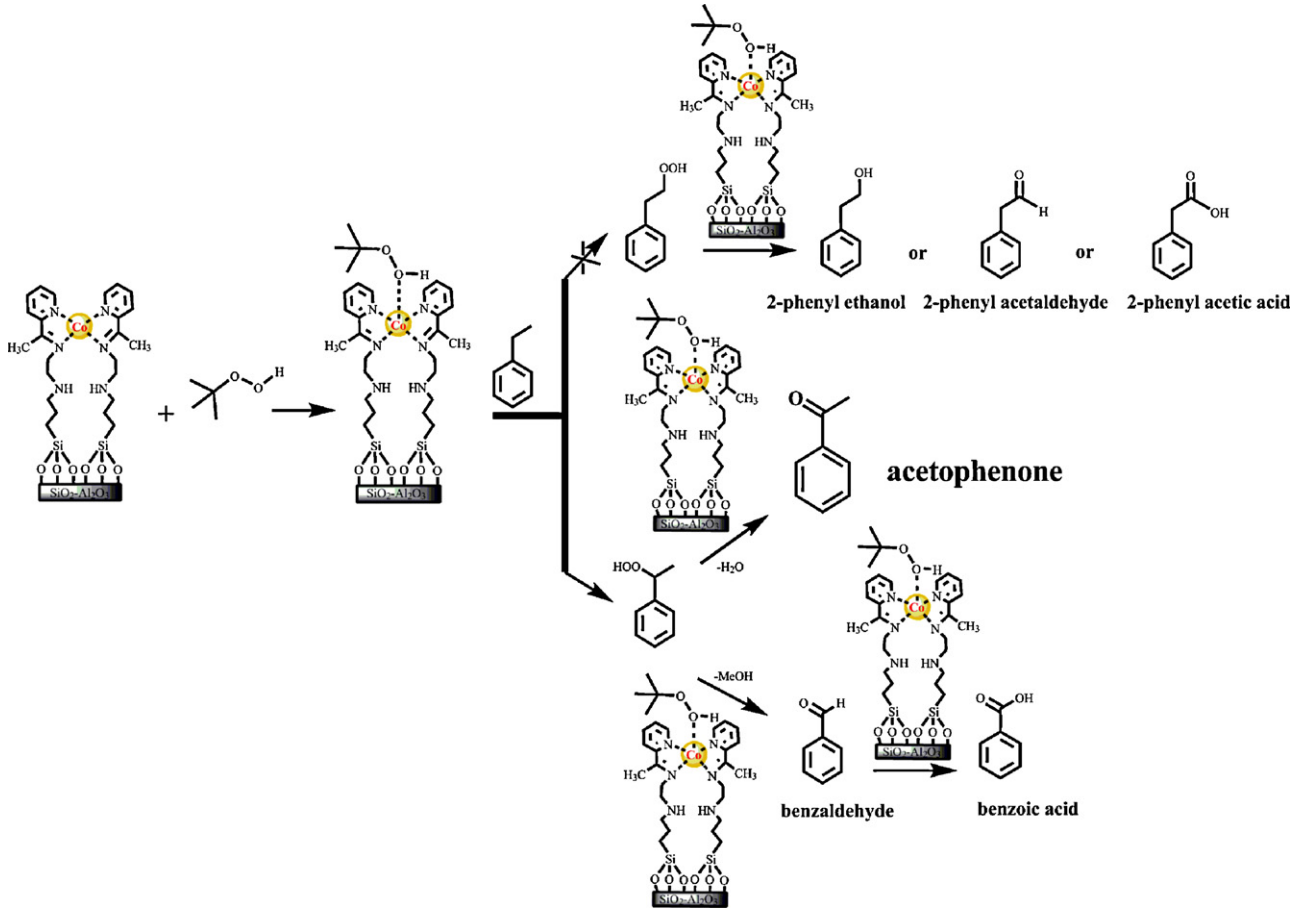

Scheme 4. Proposed mechanism for the oxidation of ethylbenzene with *tert*-butyl hydroperoxide over the Si/Al-*pr*-NH-*et*-N = methyl-2-pyridylketone-Co catalyst.

due to the low E_{pa} and charge transfer resistance that would be caused for increasing the selectivity of ethylbenzene oxidation with TBHP rather than the other complexes, which is roughly consistent with the catalytic activity and selectivity of the Co(II)–Schiff base complexes.

3.7. Proposed mechanism for the oxidation of ethylbenzene with tert-butyl hydroperoxide over the Si/Al-pr-NH-et-N = methyl-2-pyridylketone-Co catalyst

The mechanism for the oxidation of ethylbenzene with *tert*-butyl hydroperoxide over the Si/Al-pr-NH-et-N = methyl-2-pyridylketone-Co catalyst proceeded in several steps as shown in Scheme 4. TBHP is activated by coordinating with the immobilized Co(II)–Schiff base complexes, that is, the activated distant oxygen of co-coordinated TBHP reacted with ethylbenzene to yield the products. In the reaction mixture, no products (2-phenyl ethanol, 2-phenyl acetaldehyde and 2-phenyl acetic acid) were detected by GC–MS (unfavored path in Scheme 4). The oxidation of the ethylbenzene with TBHP is supposed to occur by free radical mechanism, yielding primarily ethylbenzene hydroperoxide [30]. As shown in Scheme 4, the intermediate ethylbenzene hydroperoxide can react in two different routes to form two different products, acetophenone and benzaldehyde. However, the possibility of benzoic acid formation from the over oxidation of benzaldehyde on the immobilized Co(II)–Schiff base complexes cannot be excluded.

4. Conclusion

We have described a new highly recoverable and efficient cobalt-nanocatalyst for the oxidation of ethylbenzene with TBHP without the need of any solvent at 80 °C. We have also demonstrated that the combination of an organic ligands and SiO_2–Al_2O_3 mixed-oxide resulted in an interesting synergistic effect that led to enhanced activity and selectivity of the heterogenized organocobalt nanocatalyst, the obstruction of the agglomeration of the Co(II) nanoparticles, and the generation of a durable catalyst. Among the catalysts investigated, cobalt nanoparticles immobilized over Si/Al-*pr*-NH-*et*-N = methyl-2-pyridylketone was found to be the ideal heterogeneous catalyst system for the selective oxidation of ethylbenzene. A maximum conversion (86%) and excellent selectivity (99%) were observed under milder reaction conditions with a substrate-to-oxidant ratio one time. The mutual relation of the efficiency of the prepared catalysts for ethylbenzene oxidation with the redox potential and charge transfer resistance of them were demonstrated by cyclic voltammetry (CV) and electrochemical impedance spectroscopy (EIS), respectively.

Acknowledgements

Thanks are due to the Iranian Nanotechnology Initiative and the Research Council of Isfahan University of Technology and Center of Excellence in the Chemistry Department of Isfahan University of Technology for supporting of this work.

Appendix A. Supplementary data

Supplementary data associated with this article can be found, in the online version, at doi:10.1016/j.molcata.2011.01.027.

References

[1] R.A. Sheldon, J.K. Kochi, Metal-Catalyzed Oxidation of Organic Compound, Academic Press, New York, 1981.
[2] M. Tokunaga, J.F. Larrow, F. Kakiuchi, E.N. Jacobsen, Science 277 (1997) 936.
[3] J.M. Ready, E.N. Jacobsen, J. Am. Chem. Soc. 121 (1999) 6086.
[4] T. Maeda, A.K. Pee, D. Haa, JP 7.196573, 1995;
T. Maeda, A.K. Pee, D. Haa, Chem. Abs. (1995) 256345.
[5] D.E. De Vos, P. Knops-Gerrits, R.F. Parton, B.M. Weckhuysen, P.A. Jacobs, R.A. Schoonheydt, J. Ind. Phenom. Mol. Recog. Chem. 21 (1995) 185.
[6] P.P. Paul, Prog. Inorg. Chem. 48 (1999) 457.
[7] R. Alcantara, L. Canoira, P.G. Joao, J.-M. Santos, I. Vazquez, Appl. Catal. A: Gen. 203 (2000) 259.
[8] J.-Y. Qi, H.-X. Ma, X.-J. Li, Z.-Y. Zhou, M.C.K. Choi, A.S.C. Chan, Q.-Y. Yang, Chem. Commun. (2003) 1294–1295.
[9] S. Evans, J.R. Lindsay Smith, J. Chem. Soc., Perkin Trans. 2 (2001) 174.
[10] S.S. Bhoware, A.P. Singh, J. Mol. Catal. A: Chem. 266 (2007) 118–130.
[11] Y. Ishii, T. Iwahama, S. Sakaguchi, K. Nakayama, Y. Nishiyama, J. Org. Chem. 61 (1996) 4520.
[12] M. Ghiaci, Z. Sadeghi, M.E. Sedaghat, H. Karimi-Maleh, J. Safaei, A. Gil, Appl. Catal. A: Gen. 381 (2010) 121–131.
[13] R.F. Davis, J.A. Pask, in: A.M. Alper (Ed.), "Mullite" High Temperature Oxides Part I, Academic Press, UK, 1971, p. 37.
[14] S.J. Gregg, K.S.W. Sing, Adsorption, Surface Area and Porosity, Academic Press, London, 1991.
[15] M. Ghiaci, B. Rezaei, M. Arshadi, Sens. Actuat. B 139 (2009) 494–500.
[16] H. Yang, L. Zhang, W. Su, Q. Yang, C. Li, J. Catal. 248 (2007) 204–212.
[17] L. Saikia, D. Srinivas, P. Ratnasamy, Micropor. Mesopor. Mater. 104 (2007) 225–235.
[18] R. Wang, B. Gao, W. Jiao, Appl. Surf. Sci. 255 (2009) 4109–4113.
[19] R. Mukhopadhyay, S. Bhattacharjee, R. Bhattacharyya, J. Chem. Soc., Dalton Trans. (1994) 2799.
[20] P. Karandikar, K.C. Dhanya, S. Deshpande, A.J. Chandwadkar, S. Sivasanker, M. Agashe, Catal. Commun. 5 (2004) 69–74.
[21] A.R. Silva, K. Wilson, J.H. Clark, C. Freire, Micropor. Mesopor. Mater. 91 (2006) 128–138.
[22] A.B.P. Lever, Inorganic Electronic Spectroscopy, 2nd ed., Elsevier, New York, 1984.
[23] J. Tedim, S. Patrício, R. Bessada, R. Morais, C. Sousa, M.B. Marques, C. Freire, Eur. J. Inorg. Chem. (2006) 3425–3433.
[24] M. Baltanas, S.J. DeCanio, J.R. Katzer, C. Dybowski, Acta Chim. Hung. 116 (1985) 285.
[25] W.S. Kijlstra, E.K. Poels, A. Bliek, B. Weckhuysen, R.A. Schoonheydt, J. Phys. Chem. B 101 (1997) 309–316.
[26] E. Wajnberg, L.J. El-Jaick, M.P. Linhares, D.M.S. Esquivel, J. Magn. Reson. 153 (2001) 69–74.
[27] S.S. Bhoware, S. Shylesh, K.R. Kamble, A.P. Singh, J. Mol. Catal. A: Chem. 255 (2006) 123.
[28] M. Rogovin, R. Neumann, J. Mol. Catal. A: Chem. 138 (1999) 315–318.
[29] A.J. Bard, L.R. Faulkner, Electrochemical Methods: Fundamentals and Applications, Wiley, New York, 2001.
[30] J.D. Chen, R.A. Sheldon, J. Catal. 153 (1995) 1–8.